The Arabidopsis Mutant *jason* Produces Unreduced First Division Restitution Male Gametes through a Parallel/Fused Spindle Mechanism in Meiosis II[1][W][OA]

Nico De Storme and Danny Geelen*

Department of Plant Production, Faculty of Bioscience Engineering, University of Ghent, 9000 Ghent, Belgium

In plants, whole-genome doubling (polyploidization) is a widely occurring process largely contributing to plant evolution and diversification. The generation and fusion of diploid gametes is now considered the major route of plant polyploidization. The parallel arrangement or fusion of meiosis II MII spindles (ps) is one of the most frequently reported mechanisms generating triploid offspring. Through a forward genetics screen of an Arabidopsis (*Arabidopsis thaliana*) ethyl methanesulfonate population, we identified *Arabidopsis thaliana Parallel Spindles1* (*AtPS1*), which was recently reported as a major gene implicated in the control of the ps meiotic defect. In addition, we describe the isolation and characterization of a novel allele of *JASON,* involved in male gametophytic ploidy regulation in plants. Similar to *atps1* mutants, *jason* produces more than 25% 2n pollen grains and spontaneously forms triploid offspring. By combining both cytological and genetic approaches, we demonstrate that loss of JASON causes the formation of parallel arranged and fused spindles in male MII, resulting in the production of unreduced first division restitution 2n spores. Although *JASON* encodes a protein of unknown function, we additionally show that the meiotic ps defect in *jason* is caused by a reduction in AtPS1 transcript levels, indicating that JASON positively regulates *AtPS1* expression, allowing the proper organization and orientation of metaphase II spindle plates in MII.

With the discovery of the widespread occurrence of unreduced gametes, also referred to as diplogametes, it is now believed that the major route for polyploidization happens through sexual reproduction. Here, two main mechanisms are documented: unilateral and bilateral polyploidization. In the case of unilateral sexual polyploidization, diploid gametes fuse with haploid ones, producing triploid zygotes (Mendiburu and Peloquin, 1976). Although triploid seeds generally abort, due to an altered maternal/paternal genome dosage in the endosperm (Carputo et al., 1999; Köhler et al., 2010), surviving 3x plants can function as a bridge toward tetraploid populations (Ramsey and Schemske, 1998; Husband, 2004). For Arabidopsis (*Arabidopsis thaliana*), it has been shown that this triploid bridge acts through at least one and possibly several generations of aneuploidy (Henry et al., 2005). In bilateral sexual polyploidization events, on the other hand, the fusion of two diploid gametes directly leads to a tetraploid zygote, which is potentially stable (Comai, 2005).

Unreduced gametes can be generated by a variety of cytological mechanisms. However, in plants for which the occurrence of 2n gametes has been described, unreduced pollen and/or eggs are generally formed by anomalies occurring during the meiotic cell division. These defects include abnormal spindle orientation, defective synapsis, omission of meiosis I (MI) or II (MII) and impaired cytokinesis (Bretagnolle and Thompson, 1995; Peloquin et al., 1999). Depending on the genetic outcome of these meiotic nonreduction mechanisms, resulting 2n gametes can be subdivided into two types (Hermsen, 1984): first division restitution (FDR) and second division restitution (SDR). Unreduced gametes, produced by FDR pathways, always possess the two nonsister chromatids and consequently retain equivalent levels of parental heterozygosity and epistasis. Because in SDR-type gametes, on the other hand, sister chromatids are kept together, the genetic makeup of these gametes is characterized by high levels of homozygosity. As a result, the majority of parental heterozygosity and epistatic interaction is lost (Cai and Xu, 2007).

Although production of 2n gametes is highly affected by environmental factors, several heritability assays show that this phenotype is under a strong genetic control. Genetic studies on mutant alleles responsible for the formation of 2n gametes in a number of crop species have shown that the diplogameto-

[1] This work was supported by Fonds voor Wetenschappelijk Onderzoek Flanders project G006709N.

* Corresponding author; e-mail danny.geelen@ugent.be.

The author responsible for distribution of materials integral to the findings presented in this article in accordance with the policy described in the Instructions for Authors (www.plantphysiol.org) is: Danny Geelen (danny.geelen@ugent.be).

[W] The online version of this article contains Web-only data.

[OA] Open Access articles can be viewed online without a subscription.

www.plantphysiol.org/cgi/doi/10.1104/pp.110.170415

phytic phenotype is usually monogenic (Bretagnolle and Thompson, 1995; Ramsey and Schemske, 1998).

In recent decades, several mutants producing high frequencies of 2n gametes have been identified in a number of species. In potato (*Solanum tuberosum*), the female-specific failure of cytokinesis (fc) and omission of second division (os) in megasporogenic *fc* and *os* mutants, respectively, have been shown to produce 2n eggs. Other potato mutants performing premature cytokinesis (pc) or parallel spindles (ps) during male meiosis have been shown to produce significant numbers of 2n pollen (Peloquin et al., 1999). In maize (*Zea mays*), the *elongate* (*el*) mutant causes the omission of the second division (osd) in female meiosis, leading to the formation of viable 2n eggs (Rhoades and Dempsey, 1966; Barrell and Grossniklaus, 2005). A similar osd mechanism creates unreduced megaspores in the *dyad* mutant of *Datura* (Reiser and Fischer, 1993).

Although most of these crop mutants were already identified 30 to 40 years ago, the molecular characterization of the 2n gamete-conferring genes has only recently begun. By applying both forward and reverse genetics in the model plant Arabidopsis, several genes conferring variable numbers of 2n pollen and/or eggs were identified. Ravi et al. (2008) showed that the intermediate *dyad* allele of the *DYAD/SWITCH1* gene causes rare events of female-specific meiotic nonreduction, resulting in diploid apomeiotic FDR ovules. Mutants of two other genes, *OSD* and *TAM* (*CYCA1;2*), were shown to omit the second meiotic division in both male and female sporogenesis at high frequency, resulting in the formation of both 2n pollen and eggs (d'Erfurth et al., 2009, 2010). In contrast, loss of function of the plant-specific *Arabidopsis thaliana Parallel Spindles1* (*AtPS1*) gene causes male-specific meiotic aberrations, leading to the formation of diploid pollen grains. Here, defects in spindle orientation at MII (parallel spindles) frequently cause the reallocation of already separated nonsister chromatids into dyads and triads, resulting in the formation of FDR diploid spores (Andreuzza and Siddiqi, 2008; d'Erfurth et al., 2008). A similar male-specific dyad-triad phenotype was recently observed in another mutant, called *jason* (Erilova et al., 2009). However, although it was proposed that the *jason* mutant produces diploid SDR pollen grains through a male-specific meiotic restitution mechanism, little is known about the exact mechanism controlling this meiotic aberration.

In this study, an ethyl methanesulfonate (EMS)-mutagenized Arabidopsis M2 population was screened for mutants producing diploid pollen grains. We here identify a new allele of *AtPS1,* encoding a protein implicated in controlling the spindle organization/positioning in MII. Additionally, we describe the isolation and characterization of a new allele of *JASON,* also involved in the male-specific formation of unreduced pollen in plants. We demonstrate that loss of JASON causes the production of FDR diploid pollen grains, specifically caused by a parallel/fused spindle-like phenotype at MII. Double mutant phenotyping and quantitative real-time (qRT)-PCR expression analyses further demonstrated that JASON positively regulates the expression of *AtPS1* in male sporogenesis, indicating that the meiotic restitution phenotype in *jason* mutants is caused by the loss of AtPS1 functionality.

RESULTS

Identification of New *jason* and *atps1* Alleles

Plants having higher basic ploidy levels generally produce pollen grains that are significantly larger (Bretagnolle and Thompson, 1995). This so-called pollen ploidy-size correlation was validated in Arabidopsis (ecotype Columbia [Col-0]). On average, the volume-derived diameter of a mature Arabidopsis pollen grain amounts to 21.5 μm for diploid, 27.5 μm for tetraploid, and 33.6 μm for octaploid Col-0 lines, closely corresponding to the diameter values obtained by two-dimensional pollen image analysis (Supplemental Fig. S1; Supplemental Table S1). Based on these significant pollen diameter differences, monitoring pollen size in Arabidopsis allowed the discrimination of haploid, diploid, and tetraploid pollen grains (Supplemental Fig. S1D).

In a screen for 2n pollen-producing mutants, pollen size measurements were performed on 4,800 EMS-mutagenized M2 Arabidopsis plants. Fourteen plants producing more than 20% of larger pollen grains were identified, with two lines having a similar distinctive pollen size distribution (Fig. 1, B and C). Both lines, 9-4 43 (Fig. 1B) and 4-4 28 (Fig. 1C), produced a bimodal pollen size distribution, with the low and the high value peaks corresponding to the sizes of haploid and diploid pollen grains, respectively (Supplemental Fig. S1D). To validate the increased gametophytic ploidy level in the larger pollen grains, nuclear DNA staining was performed using 4′,6-diamino-phenylindole (DAPI). Normal-sized pollen grains in both lines 9-4 43 (Fig. 1E) and 4-4 28 (Fig. 1G) showed nuclei configuration and sperm-staining intensity similar to the wild type (Fig. 1D). Larger pollen grains clearly showed enlarged sperm cells and vegetative nuclei (Fig. 1, F and G), confirming the higher DNA content of these mutant spores.

To identify the mutation in both 4-4 28 and 9-4 43 lines, an F2 mapping population was created. Based on the lack of phenotype in the heterozygous F1 population and the one-quarter segregation in the F2 population, both alleles were shown to be recessive sporophytic mutations at single nuclear loci. Low-resolution mapping and subsequent complementation testing revealed that mutant 4-4 28 is allelic to *AtPS1* (At1g34355) and mutant 9-4 43 is allelic to *JASON* (At1g06660). Sequence comparison showed that in line 4-4 28, the deletion of one guanine (position 1,253,780) in the third exon of the *AtPS1* locus causes the indirect

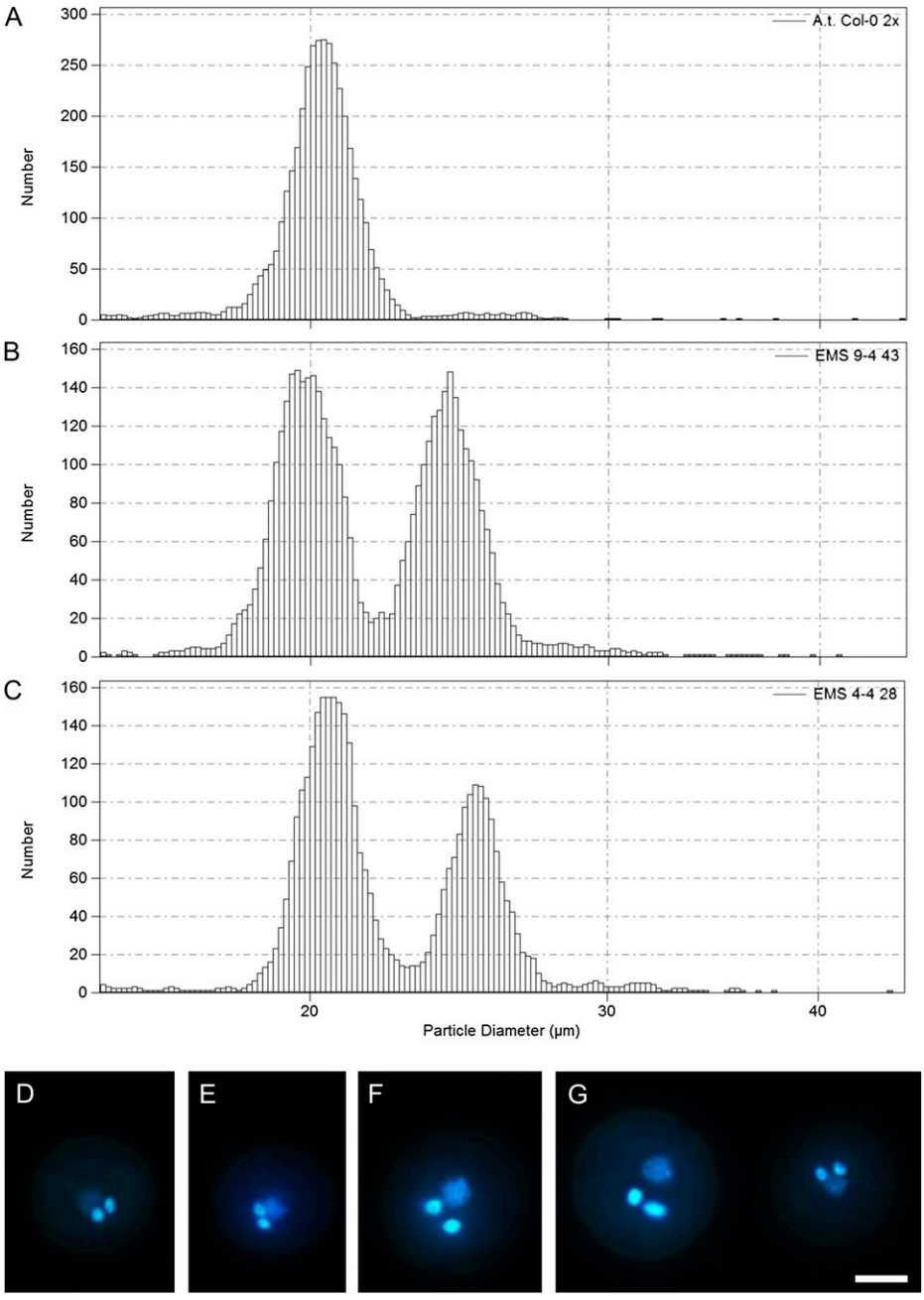

Figure 1. Pollen size distribution and nuclear DNA staining in two larger pollen mutants. A to C, The histograms represent the distribution of the volume-derived main diameter of pollen grains harvested from diploid wild-type Col-0 (A) and EMS-mutagenized 9-4 43 (B) and 4-4 28 (C) lines. D to G, Nuclear DNA staining (DAPI) of mature pollen grains isolated from diploid wild-type Col-0 (D) and EMS 9-4 43 (E and F) and EMS 4-4 28 (G) plants. The two brightly fluorescent nuclei in the tricellular pollen grains correspond to the two sperm cells; the other less condensed nucleus is the vegetative nucleus. Larger pollen grains clearly contain larger sperm nuclei in both mutants. Bar = 10 μm.

formation of a premature stop codon 17 bp downstream (Supplemental Fig. S3B). In mutant 9-4 43, a G-to-A transition (position 2,038,833) in the fourth exon of the *JASON* open reading frame causes the direct formation of a premature stop codon (TGG to TGA), generating a predicted truncated protein of 138 amino acids (Supplemental Fig. S3A).

Similarly to AtPS1, loss of JASON has been shown to cause the production of unreduced male gametes (Erilova et al., 2009). However, in contrast to AtPS1, the mechanism by which these 2n pollen are formed is largely unknown. Therefore, we focused on the *jason* mutant.

The *jason* Mutant Produces Diploid Male Gametes Leading to Triploid Progeny

The newly isolated *jason* mutant appeared highly fertile, producing a significant subpopulation of triploid progeny plants (Table I). As we did not detect any tetraploid offspring, we assumed that only male gametogenesis was affected. The successful formation of triploid plants among the progeny of a "2x wild-type (M) $\times$ 2x mutant (P)" cross, which was not observed in the reciprocal cross (data not shown), provided further evidence for the male-specific formation of diploid gametes. The additional observation of a subpopula-

Table I. *Formation of polyploid offspring in two larger pollen mutants*
Values shown are percentages. N, Number of plants analyzed.

Plant	Larger Pollen		Seed Germination		Progeny Plants			
	Mean	SD	Mean	SD	N	2×	3×	4×
Col-0 wild type	3.1	1.2	96.3	3.5	121	100	0	0
EMS 9-4 43	37.9	8.6	85.0	10.2	186	71	29	0
EMS 4-4 28	39.6	9.8	84.2	11.9	109	76.2	23.8	0

tion of larger seeds, comparable to the size of triploid seeds having a 1:2 maternal:paternal genomic dosage ratio, in the *jason* mutant is in line with the proposed unilateral sexual polyploidization mechanism through the formation of diploid male gametes (Supplemental Fig. S2; Scott et al., 1998).

To validate the gametophytic haplo-diplo ploidy distribution of the *jason* pollen population, a flow cytometric determination of the sperm DNA content was performed. As shown in Figure 2 (A–C), the *jason* mutant produces sperm cells containing either the haploid or the diploid ploidy level. Together with the DAPI staining results and the presence of triploid offspring, these data indicate that the enlarged sperms in the larger pollen grains are diploid.

An advanced quantification of the male gametophytic chromosome number was performed by crossing the pWOX2-CENH3-GFP construct into the *jason* mutant background. This construct selectively labels the microspore centromeres and thus allows the in

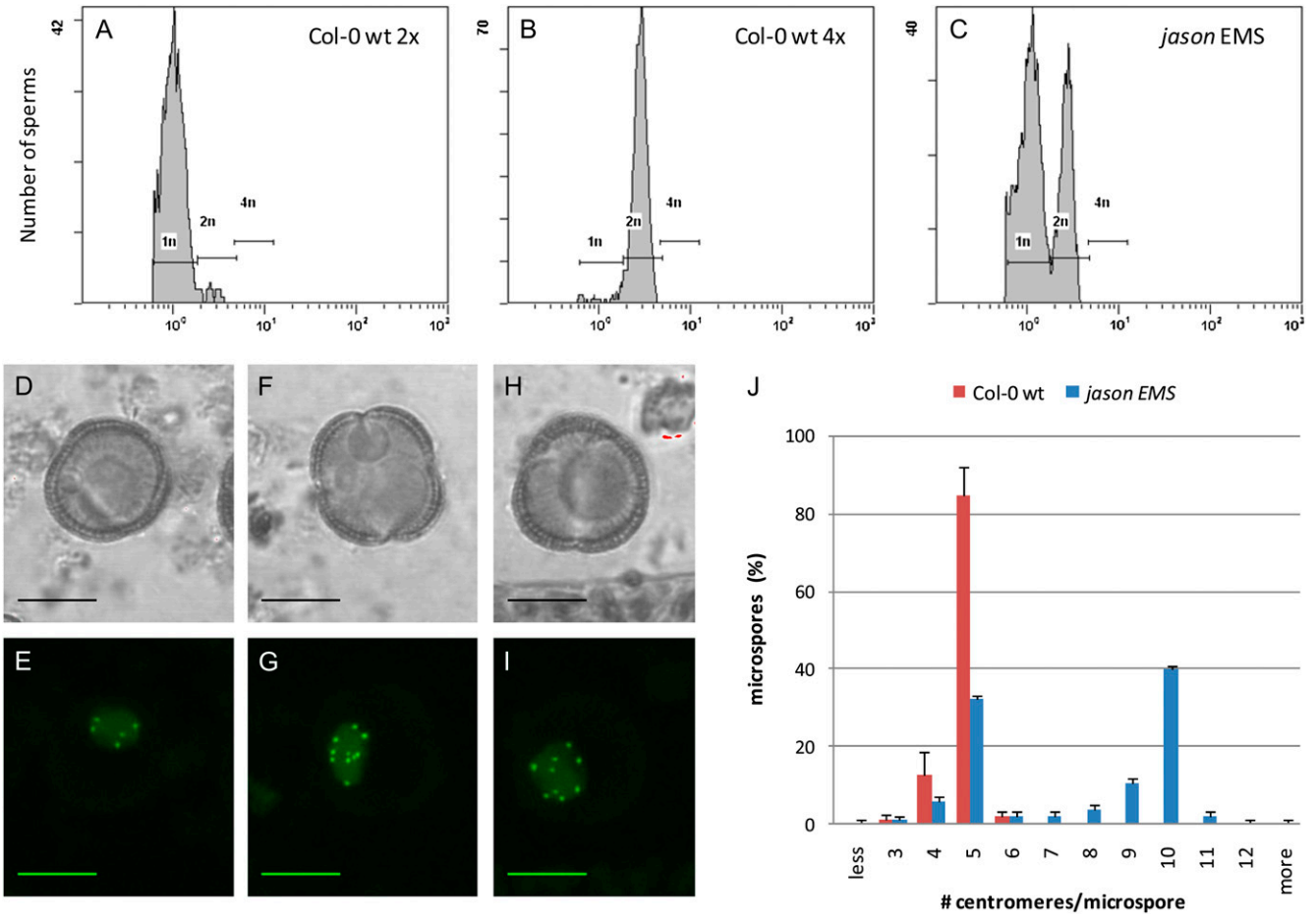

Figure 2. The *jason* mutant (EMS 9-4 43) produces diploid spores. A to C, Flow cytometric determination of the DNA content of sperm nuclei isolated from diploid wild-type (wt) Col-0 (A), tetraploid wild-type Col-0 (B), and *jason* EMS mutant (C) plants. The latter produces both haploid and diploid pollen grains. D to I, Centromere visualization in unicellular microspores of the *jason* EMS mutant enabled by introgression of the pWOX2-CENH3-GFP construct. Representative images show microspores having five (D and E), 10 (F and G), and nine (H and I) centromeric dots. Bars = 5 μm. J, Histogram showing the variability in the number of centromeric dots observed in microspores isolated from diploid Col-0 wild-type and *jason* EMS mutant plants.

vivo counting of the chromosomes in the developing male gametophyte (Supplemental Fig. S4; Chen et al., 2009). In unicellular microspores harvested from a diploid wild type, typically five centromeric dots were observed (Fig. 2J), which is consistent with the expected number of chromosomes in the haploid male gamete. The infrequent observation of four or three centromeric dots in wild-type microspores was mostly due to an overlay, a colocalization, or a differential CENH3 loading of two or more centromeres (Supplemental Fig. S4B). In contrast to the wild type, the *jason* mutant produces microspores having a highly variable number of centromeres, ranging from three to 11 (Fig. 2J). The majority of the *jason* microspores, however, contained either five or 10 centromeric dots (Fig. 2, D–I), reflecting the preferential formation of stable euploid male gametes.

In brief, these data demonstrate that the *jason* mutant, similar to *atps1*, produces triploid progeny plants through the formation of euploid 2n spores.

Diploid Gametes in the *jason* Mutant Are Generated by a Defect in Male Meiosis II

In Arabidopsis male meiosis, subsequent reductional and equational divisions normally result in the formation of a group of four haploid spores, called a tetrad. Indeed, in wild-type diploid plants, almost 100% tetrads were observed (Fig. 3A), reflecting the stable chromosome segregation in wild-type meiosis. The rare observation of only three microspores is presumably due to the escape or superposition of one of the four spores. In the *jason* EMS mutant, however, next to the tetrads (Fig. 3B), a high frequency of dyads (Fig. 3D) and triads (Fig. 3C) was observed, confirming that the diploid microspores in *jason* are produced by a defect in meiotic chromosome segregation.

A similar conclusion was made from the *jason/qrt1* (for *quartet1*) double mutant. By knocking out QRT1, the pollen mother cell wall surrounding the meiotic tetrad is not fully degraded, keeping the four spores together throughout the complete gametophytic developmental program (Rhee and Somerville, 1998; Francis et al., 2006). That way, mature pollen grains in the *qrt1* background are always released in groups of four (Fig. 3E), reflecting the tetrahedral outcome of the meiotic cell division. When we combined the *qrt1* mutation with the *jason* mutation, however, next to the tetrads (Fig. 3F), also dyad and triad (Fig. 3G) configurations were observed, providing direct evidence that mature *jason* 2n pollen grains were generated by a defect in meiotic cell division.

To determine the exact mechanism by which dyads and triads are formed in the *jason* mutant, meiotic chromosome behavior was investigated using the well-established chromosome spreading technique (Ross et al., 1996). Meiosis I in the *jason* mutant (Fig. 4, J–M) progresses normally and indistinguishably from the wild type (Fig. 4, A–F). Following chromosome condensation and crossover formation in prophase I (Fig. 4, A–C, J, and K), the metaphase I spindle aligns the five bivalents at the equatorial plane (Fig. 4, D and L) and subsequently segregates the homologs toward the poles at anaphase I (Fig. 4E), leading to two polar sets of five chromosomes (Fig. 4, F and M) at the end of MI. Starting from the second meiotic division, however, meiotic chromosome behavior in the *jason* mutant starts to deviate from the wild type. Following interkinesis, the two polar sets of five chromosomes normally align along two well-separated, perpendicularly orientated metaphase II plates (Fig. 4G), subsequently leading to the formation of four groups of five chromatids at the end of telophase II (Fig. 4, H and I). In *jason* meiocytes, however, chromosome spreading

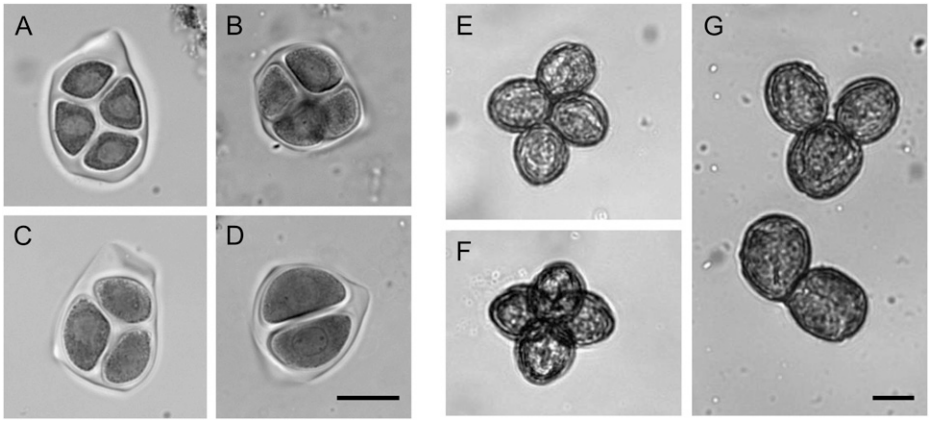

Figure 3. The *jason* EMS mutant produces both dyads and triads instead of tetrads as meiotic outcome. A to D, While meiosis in diploid wild-type plants results in a tetrad of four haploid microspores (A), the *jason* mutant also produces significant numbers of dyads and triads (B–D). E to G, By introgressing the *qrt1* mutation in the *jason* EMS mutant background, meiotic product configurations were maintained during male gametophyte development. While in a normal *qrt1* line only tetrads were observed (E), dyad/triad configurations were also observed in the *jason/qrt1* double mutant (F and G) at the end of pollen maturation. Bars = 10 μm.

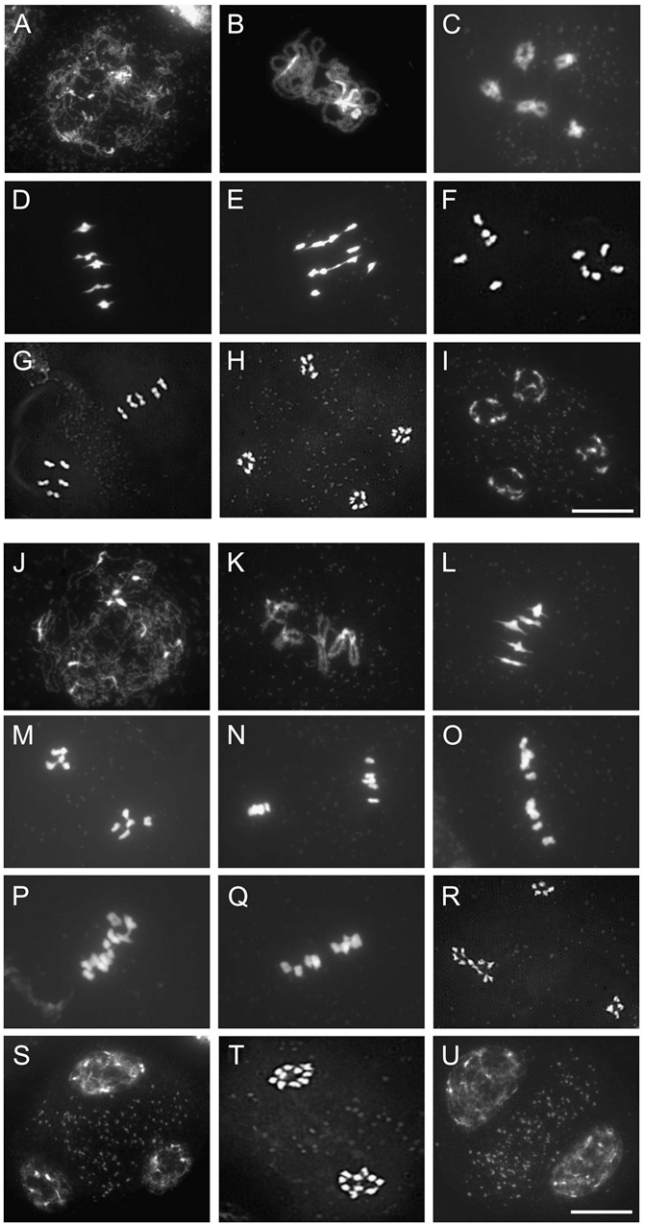

Figure 4. Meiotic chromosome behavior in diploid wild-type Col-0 (A–I) and the *jason* EMS mutant (J–U). The meiotic stages shown here are leptotene (A and J), pachytene (B), diakinesis (C and K), metaphase I (D and L), anaphase I (E), telophase I (F and M), metaphase II (G and N–Q), telophase II (H, R, and T), and the tetrad stage (I, S, and U). In wild-type meiosis, metaphase II spindle plates are oriented in a perpendicular way (G), leading to a tetrad of four haploid nuclei (five chromosomes; H). In the *jason* EMS mutant, however, the orientation of metaphase II plates is frequently parallel (O) or fused (P and Q), resulting in the formation of dyads and triads containing diploid daughter nuclei (10 chromosomes; R and T). Bars = 10 μm.

revealed that the organelle band, which is normally formed during meiotic interkinesis and distinctly persists throughout the second division (Fig. 4G), is mostly partially or completely lost (Fig. 4, N–Q), resulting in a physical nonseparation of the two daughter nuclei at the start of MII. As a consequence, the two spindle plates in *jason* MII are not always clearly separated (Fig. 4O), leading to the rejoining of the (already separated) homologs in one MII spindle plane (Fig. 4, P and Q). Subsequent segregation of sister chromatids at anaphase II consequently mimics a "mitotic-like" division, resulting in the formation of either dyads (Fig. 4, T and U; two sets of 10 chromosomes) or triads (Fig. 4, R and S; two sets of five chromosomes and one set of 10 chromosomes), which is consistent with previous findings.

Diploid *jason* Pollen Grains Retain High Levels of Parental Heterozygosity

According to the genetic outcome of the unreduced gametes, 2n pollen-producing mutants can be classified either as FDR or SDR (Bretagnolle and Thompson, 1995). In order to genotype the diploid pollen grains of a heterozygous *jason* mutant, triploid progeny plants were assayed using trimorphic molecular markers (polymorphic for Col-0, Landsberg *erecta* [L*er*], and Wassilewskija [Ws]; Supplemental Table S3). Plants homozygous for the *jason* allele and heterozygous for one or more trimorphic markers were selected out of the F2 mapping population (Col-0/L*er* background) and used as a pollen donor to fertilize Ws diploid plants. Subsequent genotyping of both diploid and triploid progeny plants, using the corresponding markers, allowed us to determine the genetic makeup of the respective haploid and diploid *jason* pollen grains.

As expected, markers in diploid offspring plants always produced two amplicons: one Ws band originating from the homozygous maternal line and one Col-0 or L*er* band originating from the heterozygous paternal line. For most markers, the segregation of the paternal polymorphism in the diploid progeny plants closely approached the expected 1:1 ratio (Table II).

Genotyping triploid offspring plants using centromere-linked trimorphic markers (ciw11 and nga76) always resulted in the presence of three amplicons (Table II): one Ws polymorphism originating from the female parent and two polymorphisms (Col-0 and L*er*) originating from the male parent. This demonstrates that the diploid pollen grains produced by the *jason* mutant fully retain the parental heterozygosity at genomic regions close to the centromere (100% for both markers). At loci more distantly located from the centromere (markers nga6 and nga151), genotypic characterization of the triploid progeny plants showed that parental heterozygosity was occasionally lost in the 2n pollen grains (heterozygosity of 48.1% and 78.6%, respectively; Table II). This observation is consistent with the presence of normal recombination in *jason* MI (Fig. 4, K and L).

In brief, these data demonstrate that diploid pollen grains produced by the *jason* mutant systematically confer high levels of parental heterozygosity: 100% at

Table II. *Genotyping of jason diploid pollen grains using trimorphic markers close to the centromere (ciw11 and nga76) and markers more distantly positioned from the centromere (nga6 and nga151)*

Values shown are percentages. N, Number of progeny plants analyzed; Het, heterozygous Col-0/L*er*.

Chromosome	SSLP	Haploid Pollen				Diploid Pollen			
		N	Col-0	Het	L*er*	N	Col-0	Het	L*er*
III	ciw11	7	42.9	0.0	57.1	20	0.0	100.0	0.0
	nga6	9	66.7	0.0	33.3	27	33.3	48.1	18.5
V	nga76	9	44.4	0.0	55.6	29	0.0	100.0	0.0
	nga151	7	22.2	0.0	77.8	28	0.0	78.6	21.4

the centromeres and decreasing levels toward the telomeres; thus, they are considered FDR.

Parallel/Fused Spindles in *jason* Meiosis II as a Meiotic Restitution Mechanism

Based on the cytological alterations observed in *jason* MII and the FDR nature of the 2n pollen generated, we assumed that the mechanism leading to dyad/triad formation in the *jason* mutant is consistent with the formation of parallel and/or fused spindles in MII. To validate this, meiotic spindle organization in the *jason* mutant was examined by immunolocalization using an α-tubulin antibody. In wild-type meiosis, the perpendicular orientation of the two metaphase II spindle planes (Fig. 5A) always leads to the formation of four distinct sets of five chromatids at the end of meiosis. In the *jason* mutant, however, the two MII spindle planes were frequently disoriented, resulting in the formation of parallel, fused, or tripolar spindles (Fig. 5, B–D). As a consequence, homologous nonsister chromatids, which were already separated in MI, are reallocated in telophase II, resulting in the formation of dyads and triads at the end of MII.

The formation of parallel/fused spindles in MII typically leads to the production of balanced dyads (two sets of 10 chromosomes) at the end of meiosis, irrespective of the preceding homolog segregation at MI. This means that the ps mechanism inherently nullifies any unbalanced chromosome distribution at MI, for example, induced by *atspo11-1-3*, restoring the production of balanced dyads at the end of MII. To validate this in the *jason* mutant, a double *jason/atspo11-1-3* mutant was constructed. Complete loss of double strand break formation in *atspo11-1-3* meiosis typically causes the formation of 10 univalents (instead of five bivalents) at metaphase I (Fig. 6, B and C), frequently leading to an unbalanced chromosome segregation at the end of MI (Fig. 6D). Subsequent separation of sister chromatids in MII consequently results in the formation of unbalanced tetrads and, due to the presence of lagging chromosomes, also in polyads having more than four nuclei (Fig. 6, F–I). As expected, the double *jason/atspo11-1-3* mutant also showed the presence of 10 univalents at metaphase I (Fig. 6, K and L), leading to an unbalanced chromosome distribution at telophase I (Fig. 6M). However, in MII, separation and segregation of sister chromatids, although originating from unbalanced sets of homolog chromosomes, resulted in the formation of balanced dyads (two sets of 10 chromosomes; Fig. 6, P, Q, and S), confirming the presence of parallel/fused spindles in *jason* MII. Next to dyads, the double *jason/atspo11-1-3* mutant also produced significant numbers of triads (Fig. 6, R and T) and tetrads (Fig. 6U). Tetrads, as expected, were almost all unbalanced. Triads, on the other hand, were characterized by one euploid set of 10 chromosomes, produced by a unipolar reallocation of chromatids, and two sets of variable chromosome numbers, reflecting the unbalanced chromosome distribution in MI.

Together, these data demonstrate that the *jason* mutant produces diploid male gametes through the formation of parallel/fused spindles at MII.

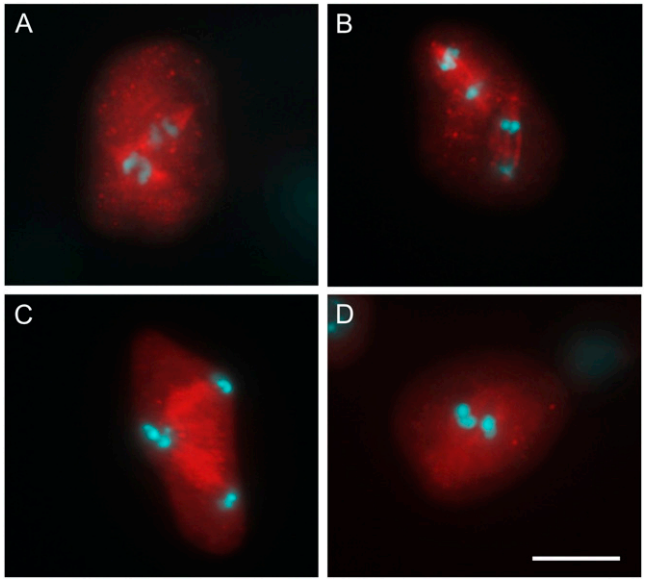

Figure 5. Orientation of spindle planes in male MII. In wild-type meiosis, metaphase II spindles are always oriented in a perpendicular way (A), allowing the formation of a tetrahedron-shaped tetrad. In *jason* male meiocytes, however, orientation of MII spindle planes was highly aberrant, showing parallel/fused and tripolar spindles (B–D), leading to meiotic dyads and triads, respectively. Microtubules were stained by immunolocalization (red) and chromosomes by DAPI (blue). Bar = 5 μm.

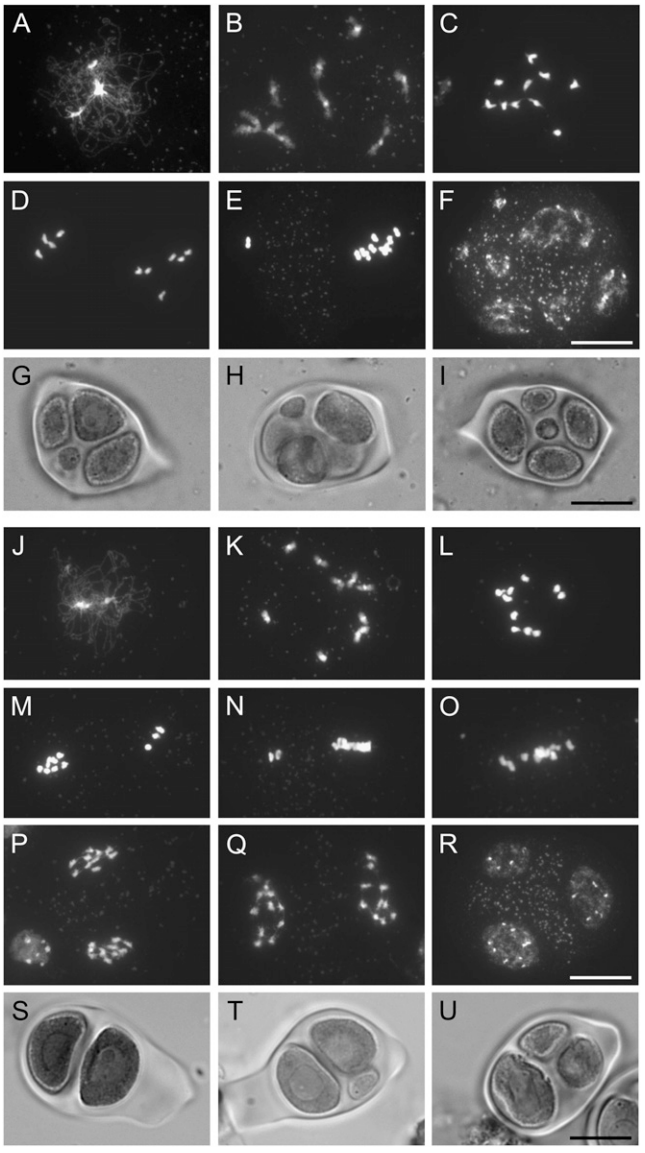

Figure 6. Meiotic chromosome behavior in *atspo11-1-3* single mutants and *jason/atspo11-1-3* double mutants. Meiotic stages shown here are leptotene (A and J), diakinesis (B and K), metaphase I (C and L), telophase I (D and M), metaphase II (E and N–O), telophase II (P and Q), and tetrad stage (F–I and R–U). Due to the complete lack of double strand break formation in the *atspo11-1-3* mutant, 10 univalents are formed at metaphase I (B, C, and K–L), leading to an unbalanced chromosome distribution in MI (D and M). As a result, meiosis produces unbalanced tetrads and polyads (F–I). By introgressing *jason* into the *atspo11-1-3* background, however, the unbalanced chromosome distribution at MI is nullified in MII (O), leading to the formation of balanced dyads (2 × 10 chromatids; P and Q). Bars = 10 μm.

JASON Positively Regulates the Level of *AtPS1* Transcripts in Early Flower Buds

Similar to *jason*, mutations in *AtPS1* also produce high numbers of FDR unreduced microspores through a parallel/fused spindles mechanism at MII (d'Erfurth et al., 2008). Moreover, frequencies of larger pollen grains (Fig. 7A), dyad/triad formation (Fig. 7B), and seed morphology (Supplemental Figs. S2 and S5B) were shown to be highly similar in both mutants, suggesting that both genes are involved in the same molecular pathway.

To check this hypothesis, a *jason/atps1* double mutant was created by combining the *jason* and *atps1* T-DNA insertion mutants described previously (d'Erfurth et al., 2008; Erilova et al., 2009). Pollen size measurements demonstrated that the 2n pollen frequency in the *jason/atps1* double mutant was significantly higher compared with the level in both single mutants (Fig. 7A). This enhanced phenotype was caused by an increased production of dyads together with a concomitant decrease of tetrads and triads at the end of MII (Fig. 7B). Based on the increased production of 2n pollen grains in the *jason/atps1* double mutant, higher frequencies of triploid progeny plants were expected. Indeed, flow cytometric ploidy analyses showed that the frequency of triploid plants in the double mutant (34.8%) was higher compared with frequencies observed in both *jason* and *atps1* single mutants (29% and 23.8%, respectively; Supplemental Fig. S5A). As triploid seeds occasionally abort, especially in the Arabidopsis Col-0 background, the higher percentage of misshapen, shriveled seeds in *jason/atps1* siliques (Supplemental Fig. S5B) indicated a higher level of triploid seed abortion, explaining the relatively low frequency of triploid progeny plants in the double mutant.

To analyze potential regulatory effects of the JASON protein on *AtPS1* gene expression and vice versa, qRT-PCR analyses using gene-specific primers were performed on RNA harvested from young meiotic flower bud material of both single and double *jason* and *atps1* mutants. The *JASON* transcript was not detected in both single *jason* T-DNA and double *jason/atps1* mutant plants (Fig. 8A). In the single *atps1* T-DNA mutant, on the other hand, a significant increase in *JASON* expression was observed, indicating that AtPS1 potentially suppresses the expression of JASON in young (meiotic) flower buds. Expression of *AtPS1* was monitored using two gene-specific primer pairs: AS1 detects the 5′ end of the *AtPS1* transcript, and RT4 is specific to the 3′ end (Supplemental Fig. S3B). Using the latter primer set, a complete loss of the full-length *AtPS1* transcript in the *atps1* mutant was demonstrated (Fig. 8B). *AtPS1* expression quantification using the 5′-specific primer set, however, showed that a small amount of *AtPS1* transcript was still present in *atps1* meiotic buds, suggesting that a minor fraction of the *AtPS1* transcripts was not fully processed. More surprisingly, in both *jason* single mutants, also a significant decrease in *AtPS1* expression was observed. This indicates that JASON either positively regulates the expression of *AtPS1* or prevents the degradation of the corresponding transcript in young (meiotic) flower buds. Moreover, because for all lines the penetrance of the 2n pollen phenotype (dyad formation) was reflected by the decrease in *AtPS1* expression (Figs. 7A

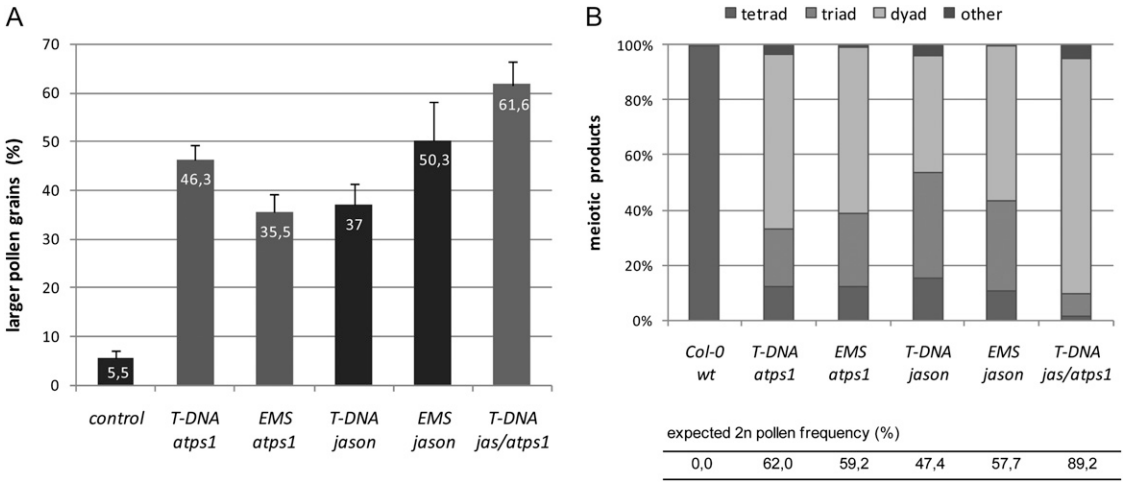

Figure 7. Quantitative variation in larger pollen grain production (A) and dyad/triad formation (B) in single and double *jas/atps1* mutants. The frequency of dyads, triads, and tetrads and the predicted percentage of diploid pollen were quantified for each mutant (B). The actual percentages of larger pollen grains (A), as an indicator for 2n pollen, were consistently lower compared with the predicted level.

and 8B), there appeared to be a close correlation between the loss of *AtPS1* expression and the frequency of dyad formation. More specifically, loss of the 5′ end of the *AtPS1* transcript showed stronger correlation with the phenotype compared with levels of the 3′ end (Fig. 8B).

Although the phenotyping of both single and double *jason/atps1* mutant lines together with the qRT-PCR expression data already suggested a meiosis-specific function of JASON regulating *AtPS1* expression, potential interregulatory effects outside meiosis could not be excluded. To address this issue, we monitored *AtPS1* and *JASON* expression in nonmeiotic plant tissue (postmeiotic flower buds and rosette leaf material) harvested from both *jason* and *atps1* EMS and T-DNA mutants using RT-PCR. As shown in Figure 8 (C and D), both *AtPS1* and *JASON* transcripts are present in somatic leaf and flower material, clearly demonstrating that both genes are not exclusively expressed in meiotic cells. In *atps1* somatic material, next to the expected loss of the *AtPS1* transcript, also reduced levels of *JASON* were observed, suggesting a promotive effect of AtPS1 on *JASON* expression in somatic cells. Unlike observations in young meiotic flowers, however, *AtPS1* transcript levels in *jason* somatic tissue were not altered (Fig. 8, C and D), suggesting that JASON does not modulate *AtPS1* expression in mitotic cells and specifically regulates *AtPS1* expression in meiotic cells.

Altogether, these data show that the *jason* mutant produces diploid pollen grains through a reduction in *AtPS1* transcript levels in meiotic flower buds.

DISCUSSION

In this study, a pollen size-based screen was used to identify Arabidopsis EMS mutants producing diploid pollen grains. In agreement with other studies, we show that there is a clear correlation between the size of Arabidopsis pollen grains and their respective gametophytic ploidy level (Ramanna, 1979; Jansen and Nijs, 1993; Altmann et al., 1994; Bretagnolle and Thompson, 1995; Ramsey and Schemske, 1998; Crespel et al., 2006). By means of this pollen ploidy-size correlation, we identified two new mutants producing significant numbers of diploid male gametes. Positional cloning and complementation testing revealed that mutant EMS 4-4 28 and EMS 9-4 43 are allelic to *AtPS1* and *JASON*, respectively.

d'Erfurth et al. (2008) demonstrated that lack of AtPS1 function leads to a parallel or a tripolar orientation of the two spindles in male MII, causing the formation of meiotic dyads and triads that eventually develop into FDR diploid spores (Andreuzza and Siddiqi, 2008). Mutations in the JASON gene have also been shown to cause the production of dyads and triads through a male-specific meiotic nonreduction pathway. However, in contrast to AtPS1, the mechanism by which these 2n pollen are formed is largely unknown. Erilova et al. (2009) postulated that lack of JASON causes a failure of chromatid segregation during male MII, leading to the production of SDR 2n gametes. Here, both sister chromatids of the same homolog remain at the same pole during MII, conferring high levels of homozygosity to the resulting diploid pollen grains. In our study, however, a genetic analysis demonstrated that *jason* diploid spores were systematically heterozygous in close proximity to the centromere and segregating at loci more distant, specifically pointing toward an FDR meiotic defect (Bretagnolle and Thompson, 1995). These data, together with the observation of parallel and fused metaphase II plates in meiotic cytological preparations, suggested

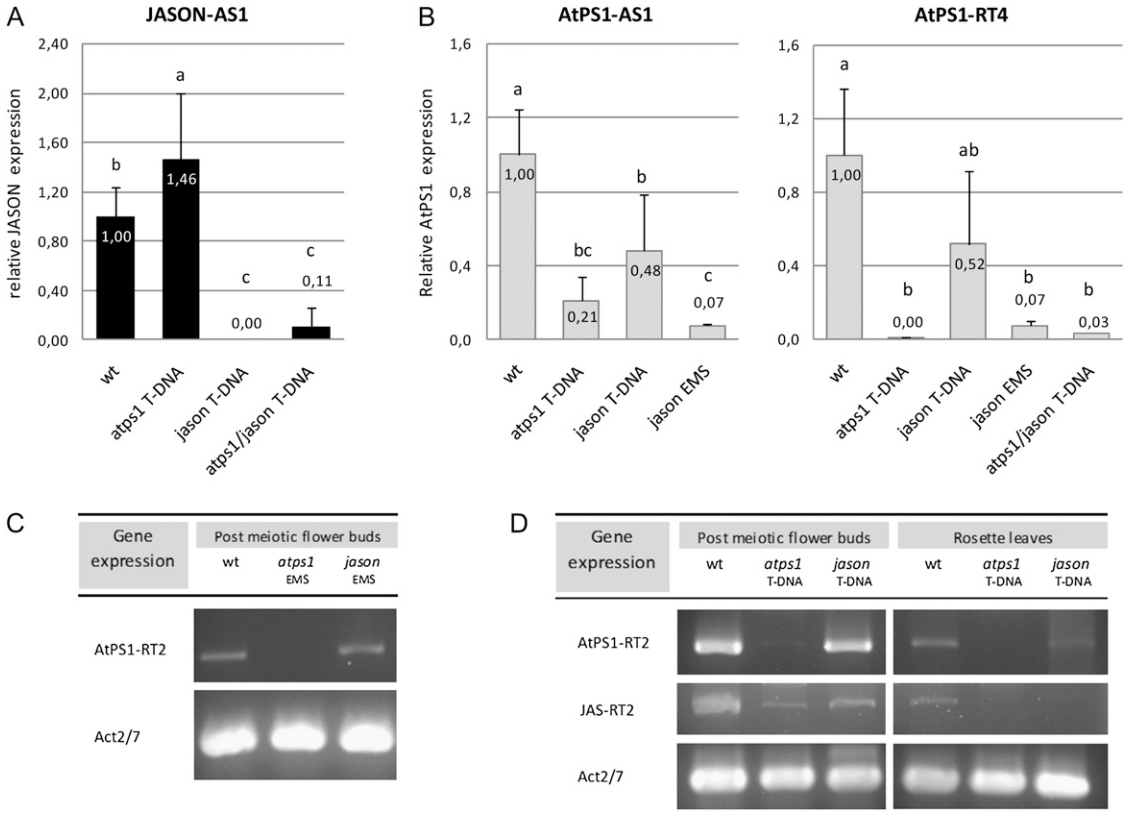

Figure 8. Differential expression of JASON and AtPS1 in the wild type (wt) and corresponding *jason* and *atps1* mutants. For quantitative expression analysis, qRT-PCR was performed on RNA harvested from young meiotic flower buds. A, Transcript levels of JASON were quantified using one gene-specific primer pair (JAS-AS1). B, For AtPS1, two gene-specific primer pairs were used, one at the 5′ end (AtPS1-AS1) and one at the 3′ end (AtPS1-RT4). Glyceraldehyde 3-phosphate dehydrogenase, Actin2, and Actin2/7 were used to normalize initial cDNA concentrations. Comparative statistics of the means were checked using a one-way ANOVA test (SPSS15). C and D, Comparative expression of JASON and AtPS1 in somatic tissues (postmeiotic flower buds and rosette leaf material) of EMS (C) and T-DNA (D) *jason* and *atps1* mutants was monitored using RT-PCR.

that *jason* dyads and triads originate from a meiotic parallel/fused spindle-type defect rather than from chromatid segregation failure. Indeed, as *jason* was demonstrated to nullify any *atspo11-1-3*-induced unbalanced chromosome segregation defect in its dyads, the formation of parallel/fused spindles in MII was established as the mechanism governing 2n spore formation in *jason*.

For the newly isolated *jason* allele, frequencies of 2n pollen grain production were very similar to the level observed in the new *atps1* mutant, closely corresponding to the level of 40% observed in the *atps1* alleles described by d'Erfurth et al. (2008). In both *jason* and *atps1* mutants, however, the frequency of mature diplopollen was significantly lower compared with the expected level based on dyad/triad production. One possible explanation is that a small fraction of the "unreduced" microspores are aneuploid, resulting in premature pollen abortion. Although the gametophytic CENH3-GFP counting analysis seemingly supported this hypothesis, confocal three-dimensional imaging showed that the observation of *jason* microspores having aneuploid chromosome numbers was mainly attributed to overlapping centromeres, insufficient CENH3-GFP loading, or asynchronous gametophytic chromosome replication/division. In meiotic chromosome spreading as well, no aneuploid dyads and triads were observed, indicating that only euploid male gametes were produced. Moreover, visualization of *jason* dyads and triads at the end of pollen development (*qrt1* background) did not show any noticeable pollen abortion, indicating that all the diploid microspores matured into viable 2n pollen grains. We thus conclude that the discrepancy between dyad/triad and 2n pollen frequency was mainly attributed to differences in counting method rather than to the hypothesized ploidy-induced pollen abortion.

Although JASON was shown to be conserved throughout the plant kingdom, containing a highly conserved C-terminal domain, the gene encodes an unknown protein without any functional annotation and no homologs in animals or yeast (Erilova et al., 2009). Similar to AtPS1, the observed spindle anomalies in *jason* male meiosis suggest a role for JASON in the organization and orientation of the spindle apparatus in meiosis. Moreover, because the parallel/fused

spindle defect in *jason* closely correlated with a sharp decrease of *AtPS1* transcript levels in young (meiotic) flower buds while *AtPS1* expression in other somatic tissues was not altered, JASON is thought to be involved in regulating the proper expression of *AtPS1* in meiotic cells, allowing the normal progression of MII. The predominant expression of *JASON* during reproductive development together with the enhanced 2n pollen phenotype in the double *jason/atps1* mutant are consistent with this meiosis-specific function. However, how JASON regulates *AtPS1* expression in meiotic cells still remains elusive.

The AtPS1 protein has two distinct domains: an N-terminal forkhead-associated (FHA) domain and a PilT N Terminus (PIN or PINc in SMART database) domain located at the C terminus. Based on homology of the latter with PINc domains of other putative meiotic genes (Swt1/C1orf26/CG7206) and SMG6, the PINc motif was hypothesized to have regulatory functions in meiotic cell cycle progression, potentially through the control of nonsense-mediated RNA decay (Clissold and Ponting, 2000; d'Erfurth et al., 2008). In our study, however, expression analyses demonstrated that loss of the 5′ end of the *AtPS1* transcript showed stronger correlation with the penetrance of the 2n pollen phenotype compared with loss of the 3′ end, indicating that the N-terminal FHA domain and not the PINc domain was considered the regulating motif controlling tetrad formation in male MII. The FHA domain is a phosphopeptide recognition motif present in a wide variety of proteins in both prokaryotes and eukaryotes (Durocher et al., 1999; Li et al., 2000). In plants, the FHA module participates in the regulation of numerous processes, including intracellular signaling, plant meristem homeostasis, DNA repair, transcription, protein degradation, and cell cycle control (Durocher and Jackson, 2002).

The tendency to produce more dyads (more parallel/fused spindles) instead of triads and tetrads with decreasing 5′ end *AtPS1* transcript levels potentially indicates that the FHA domain is involved in the proper establishment of meiotic microtubule organizing centers (MTOCs), either by regulating proper MTOC division/nucleation following MI or by controlling the meiosis-specific tetrahedral division polarity in MII. Although γ-tubulin is widely accepted as the acentriolar plant MTOC (Murata et al., 2005; Pastuglia et al., 2006), the precise mechanism controlling spindle orientation and biogenesis during the meiotic cell cycle remains elusive (Brown and Lemmon, 2007). In basal plants, meiotic MTOCs were shown to appear spatially distributed along the four plastids in prophase I, indicating a premeiotic establishment of the tetrahedral polarity of the meiotic cell through plastid division (Shimamura et al., 2004). In higher plants, however, little is known about meiotic polarity establishment (Vecchio et al., 1996).

Another hypothesis is that AtPS1 functions in establishing or maintaining the physical separation of the two daughter nuclei after MI. Following chromosome segregation in metaphase/anaphase I, the primary interzonal microtubule array is crucial in establishing a first preliminary physical separation between the two haploid nuclei (Genualdo et al., 1998; Conicella et al., 2003). Both the lack of a typical organelle band and the frequent observation of fused daughter nuclei at metaphase II in both *jason* and *atps1* mutants supports the idea that AtPS1 functions in establishing or maintaining this interzonal microtubule array. Although preliminary tubulin immunolocalization experiments did not show any clear alteration in interzonal microtubule array organization, more detailed analyses will be needed to address this issue.

CONCLUSION

In brief, the isolation of *JASON* as a major gene regulating spindle organization in MII through the control of *AtPS1* transcript levels is an important step in elucidating the molecular mechanisms regulating reductional cell division in higher plants. Moreover, as lack of JASON function, as in *atps1* mutants, causes the formation of FDR diploid pollen, both alleles can have potential applications in fundamental polyploidization research and plant breeding programs.

MATERIALS AND METHODS

Plant Materials and Growth Conditions

Following an initial in vitro seed germination (6–8 d, K1 medium), Arabidopsis (*Arabidopsis thaliana*) seedlings were cultivated in fully controlled climate chambers under the following conditions: photoperiod of 12-h day/12-h night, temperature of 20°C, and humidity less than 70%. At the start of flower initiation, photoperiod settings were changed to 16-h day/8-h night under the same conditions to stimulate flowering.

Arabidopsis diploid and tetraploid Col-0 wild-type accessions were ordered from the Nottingham Arabidopsis Stock Centre. Octaploid plants were generated by submerging 7-d-old, tetraploid Col-0 seedlings for 2 h in a 0.1% (w/v) colchicine solution. After washing with copious amounts of water, seedlings were transferred into soil. At flower initiation, the somatic ploidy level of the treated plants (P0) was determined using flow cytometry. Progeny of octaploid P0 plants were grown, and the resulting octaploid P1 plants were used for further analyses. Mutants 9-4 43 (*jason*) and 4-4 28 (*atps1*) were isolated from an M2 Arabidopsis Col-0 seed stock (Lehle Seeds) that was mutagenized using EMS. All other mutant alleles in this study, *atps1-1* (SALK _078818), *jason* (SALK _083575), *qrt1-1* (N8845), and *atspo11-1-3* (SALK_146172), were T-DNA insertion lines in the Col-0 background originating from the European Arabidopsis Stock Centre.

The pWOX2-CENH3-GFP-expressing line was constructed using the Multisite-Gateway cloning system according to the manufacturer's instructions (Invitrogen). The verified plasmid was transformed into *Agrobacterium tumefaciens* strain GV3130 and used to generate transgenic Arabidopsis Col-0 lines. Single T-DNA-carrying transgenic progeny plants were selected based on kanamycin selection and stable GFP expression following fluorescence analysis.

Ploidy Determination

The somatic ploidy level was determined using flow cytometry (Epics Altra; Beckman) based on the nuclei extraction method of Galbraith et al. (1983). Here, fresh leaf material was chopped with a sharp razor blade in 200 μL of Galbraith's buffer, and the resulting nuclei suspension was filtered through a 40-μm nylon mesh (Galbraith et al., 1983; Durbarry et al., 2005). After staining the isolated nuclei with propidium iodide (final concentration

of 10 μM), the corresponding DNA content was analyzed flow cytometrically (excitation, 488 nm; signal detection, 575 nm).

The gametophytic ploidy level of sperm cells was determined in the same way. However, extraction of the sperm cells out of the pollen grains was performed mechanically by grinding a large amount of pollen grains in 50 μL of Galbraith's buffer (30 s at 30 Retsch). After filtration through an 11-μm mesh, isolated sperm nuclei were stained using propidium iodide (final concentration of 10 μM) for flow cytometric ploidy determination.

Phenotypic Analyses

Extraction of pollen was performed by putting mature flowers in 0.5 M EDTA (pH 8.0) at gentle agitation for 5 to 10 min. After removing the flower material, the resulting pollen suspension was centrifuged for 5 min at 13,000*g* to isolate the pollen fraction in the pellet. Using this material, pollen size analysis was performed either two dimensionally using bright-field microscopy and automated image analysis or volumetrically using a cell-counting device (Multisizer II; Coulter Counter). Based on the pollen ploidy-size correlation, the frequency of higher ploidy pollen grains was estimated by selecting a pollen diameter of 23 μm, below which the pollen were classified as haploid. Pollen exceeding this diameter threshold were considered as having a higher gametophytic ploidy level.

Nuclear DNA staining of mature pollen grains was performed based on the protocol described by Durbarry et al. (2005) with minor modifications. After pollen extraction in 0.5 M EDTA, the resulting pollen pellet was fixed in 3:1 ethanol:acetic acid for 30 min, washed with distilled water, and resuspended in DAPI solution (1 μg mL^{-1}; Sigma) for 30 min. Subsequent centrifugation and additional washing steps resulted in a DAPI-stained pollen sample that was observed using fluorescence microscopy.

Analysis of meiotic outcome was performed by selecting meiotic buds based on size and shape and squashing them on a slide in a drop of 4.5% (w/v) lactopropionic orcein staining solution. Buds producing significant numbers of fully developed meiotic products were used for counting assays.

Low-Resolution Mapping

For each isolated EMS mutant, an F2 mapping population was created by crossing a diploid homozygous mutant plant (Col-0 background) with a diploid wild-type L*er* plant. Selfing of the heterozygous F1 hybrid subsequently resulted in the F2 mapping population. F2 plants showing the recessive larger pollen phenotype were selected and genotyped using Col-L*er* polymorphic simple sequence length polymorphism (SSLP) markers to establish linkage with the original Col-0 background. The resulting genomic regions with highest Col-0 linkage were then screened in silico for potential candidate genes.

Genetic Analysis

T-DNA insertion mutants (SALK) were genotyped by PCR amplification using two primer pairs: the LB-RB pair specifically amplifies the wild-type allele, and the BP-RB pair is specific to the T-DNA insertion in the gene of interest. Sequences of both primer sets with their corresponding PCR amplification settings for each mutant are listed in Supplemental Table S2.

The genotype of diploid pollen grains harvested from a heterozygous Col-0/L*er* mutant plant was determined by crossing mutant pollen onto haploid wild-type pistils of the Ws background and by genotyping the resulting triploid offspring using trimorphic SSLP markers. Primer sequences of trimorphic SSLP markers and their corresponding PCR amplification settings are listed in Supplemental Table S3.

Cytology

Chromosome behavior during meiotic cell division was visualized cytologically using the well-established chromosome-spreading technique (Jones and Heslop-Harrison, 1996) with some minor modifications. After fixation of meiotic buds in 3:1 ethanol:acetic acid, buds were rinsed twice (once in distilled water and once in citrate buffer) and incubated in an enzyme mixture consisting of 0.3% (w/v) pectolyase (Sigma) and 0.3% (w/v) cellulase (Sigma) in citrate buffer at 37°C in a moisture chamber for 1.5 h. Digested buds were subsequently rinsed and stored at 4°C in citrate buffer. A single enzyme-digested bud was transferred to a slide, macerated with a needle in a small drop of 60% acetic acid, and stirred gently on a hotplate at 45°C for 30 s The slide was then flooded with freshly made ice-cold 3:1 ethanol:acetic acid and subsequently air dried. Finally, slides were stained by adding 25 μL of DAPI (1 μg mL^{-1}) in Vectashield antifade mounting medium, mounted with a coverslip, and squashed between filter paper to remove excess stain and mounting medium.

To analyze microtubule dynamics and MII spindle orientation in male meiosis, a tubulin immunolocalization assay was performed according to the method of Mercier et al. (2001) with some minor modifications. After *m*-maleimidobenzoyl *N*-hydrosuccinimide ester treatment and fixation in 4% paraformaldehyde, inflorescences were washed in 50 mM potassium phosphate buffer (pH 8) and digested in an enzyme mixture consisting of 0.3% (w/v) pectolyase (Sigma), 0.3% (w/v) cytohelicase (Sigma), and 0.3% (w/v) cellulase (Sigma) in a humid chamber at 37°C. Enzyme-digested anthers were dissected, squashed, and fixed on a slide by freezing in liquid nitrogen. Released cells were then covered with a thin layer of 1% (w/v) gelatin, 1% (w/v) agarose, and 2.5% Glc and digested for 30 min at 37°C by using the same enzyme mix. After rinsing with potassium phosphate buffer, the immobilized cells were incubated overnight at room temperature with the rat alfa-tubulin primary antibody (0.3% [v/v]; Clone B-5-1-2; Sigma-Aldrich) in phosphate-buffered saline (PBS), 0.1% (v/v) Triton X-100, and 4.5 g L^{-1} bovine serum albumin. Cells were rinsed three times with PBS and 0.1% (v/v) Triton X-100 and treated for 3 h with 0.5% (v/v) secondary antibody (labeled goat anti-rat) at 37°C in the dark. After three rinses with PBS and 0.1% (v/v) Triton X-100, a small droplet of DAPI (2 μg mL^{-1}) in Vectashield mounting medium was added to stain the cell's chromosomes (Mercier et al., 2001).

Microscopy

Imaging of mature pollen and lactopropionic orcein-stained meiotic products and microscopic observation of cells expressing CENH3-GFP or stained for meiotic chromosome, pollen nuclei, or spindle visualization were performed using an Olympus IX81 inverted fluorescence microscope equipped with an X-Cite Series 120Q UV lamp and an Olympus XM10 camera. Confocal three-dimensional imaging of centromeric CENH3-GFP localization was performed using a Nikon A1r laser scanning microscope equipped with Axiovision software (LiMiD).

Expression Analyses

Total plant RNA was prepared using the RNeasy Plant Mini Kit with additional on-column DNaseI treatment (Qiagen). First-strand cDNA was synthesized using the RevertAid H Minus cDNA Synthesis Kit (Fermentas) according to the manufacturer's guidelines. Gene expression analysis in meiotic floral bud tissue was performed by qRT-PCR on a Stratagene MX3000 real-time PCR system using SYBR Green Master Mix. Sequences of primers used for specific amplification of JASON (AS1), AtPS1 (AS1 and RT4), and housekeeping gene transcripts together with the corresponding qRT-PCR settings are listed in Supplemental Table S4. Gene expression in somatic tissues was performed using the Qiagen OneStep RT-PCR kit according to the manufacturer's instructions. Gene-specific primers used for RT-PCR (JASON-RT2, AtPS1-RT2, and Act2/7) are also listed in Supplemental Table S4.

Supplemental Data

The following materials are available in the online version of this article.

Supplemental Figure S1. Pollen ploidy-size correlation in Arabidopsis (Col-0 background).

Supplemental Figure S2. Seed size distribution of larger pollen-producing lines.

Supplemental Figure S3. The intron/exon structure of both *JASON* and *AtPS1* genes.

Supplemental Figure S4. In vivo chromosome counting during microspore development.

Supplemental Figure S5. Triploid offspring formation and seed set in single and double *jas/atps1* mutants.

Supplemental Table S1. Descriptive statistics of ploidy-dependent pollen size parameters in Arabidopsis (Col-0 background).

Supplemental Table S2. Oligonucleotides used for T-DNA detection and genotyping.

Supplemental Table S3. Trimorphic SSLP markers used for genotyping diploid pollen grains.

Supplemental Table S4. Oligonucleotides used for qRT-PCR expression analyses.

ACKNOWLEDGMENTS

We are grateful to Monica Höfte, (Phytopathology, University of Ghent), David De Vleesschauwer (Phytopathology, University of Ghent), and Winnok De Vos (LiMiD-Hercules Foundation project AUGE/013), for technical support regarding qRT-PCR and confocal microscopy. We also thank Susan Armstrong (School of Biosciences, University of Birmingham) for helping us with the chromosome-spreading technique (EMBO Short-Term Fellowship) and helpful comments. Many thanks as well to Raphael Mercier and Laurence Cromer (INRA, Versailles) for demonstrating the immunolocalization protocol (European Cooperation in Science and Technology FA0903 Short-Term Scientific Mission) and providing *atps1* seed material.

Received December 2, 2010; accepted January 20, 2011; published January 21, 2011.

LITERATURE CITED

Altmann T, Damm B, Frommer WB, Martin T, Morris PC, Schweizer D, Willmitzer L, Schmidt R (1994) Easy determination of ploidy level in Arabidopsis thaliana plants by means of pollen size measurement. Plant Cell Rep **13:** 652–656

Andreuzza S, Siddiqi I (2008) Spindle positioning, meiotic nonreduction, and polyploidy in plants. PLoS Genet 4: e1000272

Barrell PJ, Grossniklaus U (2005) Confocal microscopy of whole ovules for analysis of reproductive development: the elongate1 mutant affects meiosis II. Plant J **43:** 309–320

Bretagnolle F, Thompson JD (1995) Tansley Review No. 78. Gametes with the somatic chromosome-number: mechanisms of their formation and role in the evolution of autopolyploid plants. New Phytol **129:** 1–22

Brown RC, Lemmon BE (2007) The pleiomorphic plant MTOC: an evolutionary perspective. J Integr Plant Biol **49:** 1142–1153

Cai XW, Xu SS (2007) Meiosis-driven genome variation in plants. Curr Genomics **8:** 151–161

Carputo D, Monti L, Werner JE, Frusciante L (1999) Uses and usefulness of endosperm balance number. Theor Appl Genet **98:** 478–484

Chen Z, Hafidh S, Poh SH, Twell D, Berger F (2009) Proliferation and cell fate establishment during Arabidopsis male gametogenesis depends on the retinoblastoma protein. Proc Natl Acad Sci USA **106:** 7257–7262

Clissold PM, Ponting CP (2000) PIN domains in nonsense-mediated mRNA decay and RNAi. Curr Biol **10:** R888–R890

Comai L (2005) The advantages and disadvantages of being polyploid. Nat Rev Genet **6:** 836–846

Conicella C, Capo A, Cammareri M, Errico A, Shamina N, Monti LM (2003) Elucidation of meiotic nuclear restitution mechanisms in potato through analysis of microtubular cytoskeleton. Euphytica **133:** 107–115

Crespel L, Ricci SC, Gudin S (2006) The production of 2n pollen in rose. Euphytica **151:** 155–164

d'Erfurth I, Cromer L, Jolivet S, Girard C, Horlow C, Sun YJ, To JPC, Berchowitz LE, Copenhaver GP, Mercier R (2010) The cyclin-A CYCA1;2/TAM is required for the meiosis I to meiosis II transition and cooperates with OSD1 for the prophase to first meiotic division transition. PLoS Genet 6: e1000989

d'Erfurth I, Jolivet S, Froger N, Catrice O, Novatchkova M, Mercier R (2009) Turning meiosis into mitosis. PLoS Biol 7: e100124

d'Erfurth I, Jolivet S, Froger N, Catrice O, Novatchkova M, Simon M, Jenczewski E, Mercier R (2008) Mutations in AtPS1 (Arabidopsis thaliana parallel spindle 1) lead to the production of diploid pollen grains. PLoS Genet **4:** e1000274

Durbarry A, Vizir I, Twell D (2005) Male germ line development in Arabidopsis: duo pollen mutants reveal gametophytic regulators of generative cell cycle progression. Plant Physiol **137:** 297–307

Durocher D, Henckel J, Fersht AR, Jackson SP (1999) The FHA domain is a modular phosphopeptide recognition motif. Mol Cell **4:** 387–394

Durocher D, Jackson SP (2002) The FHA domain. FEBS Lett **513:** 58–66

Erilova A, Brownfield L, Exner V, Rosa M, Twell D, Scheid OM, Hennig L, Kohler C (2009) Imprinting of the Polycomb group gene MEDEA serves as a ploidy sensor in Arabidopsis. PLoS Genet 5: e1000663

Francis KE, Lam SY, Copenhaver GP (2006) Separation of Arabidopsis pollen tetrads is regulated by QUARTET1, a pectin methylesterase gene. Plant Physiol **142:** 1004–1013

Galbraith DW, Harkins KR, Maddox JM, Ayres NM, Sharma DP, Firoozabady E (1983) Rapid flow cytometric analysis of the cell cycle in intact plant tissues. Science **220:** 1049–1051

Genualdo G, Errico A, Tiezzi A, Conicella C (1998) α-Tubulin and F-actin distribution during microsporogenesis in a 2n pollen producer of Solanum. Genome **41:** 636–641

Henry IM, Dilkes BP, Young K, Watson B, Wu H, Comai L (2005) Aneuploidy and genetic variation in the Arabidopsis thaliana triploid response. Genetics **170:** 1979–1988

Hermsen J (1984) Mechanisms and genetic implications of 2n-gamete formation. Iowa State J Res **58:** 421–434

Husband BC (2004) The role of triploid hybrids in the evolutionary dynamics of mixed-ploidy populations. Biol J Linn Soc Lond **82:** 537–546

Jansen RC, Nijs APMD (1993) A statistical mixture model for estimating the proportion of unreduced pollen grains in perennial ryegrass (*Lolium perenne* L.) via the size of pollen grains. Euphytica **70:** 205–215

Jones G, Heslop-Harrison J, eds (1996) Classical and Molecular Cytogenetics of Arabidopsis thaliana. Oxford University Press, Oxford

Köhler C, Mittelsten Scheid O, Erilova A (2010) The impact of the triploid block on the origin and evolution of polyploid plants. Trends Genet **26:** 142–148

Li J, Lee GI, Van Doren SR, Walker JC (2000) The FHA domain mediates phosphoprotein interactions. J Cell Sci **113:** 4143–4149

Mendiburu AO, Peloquin SJ (1976) Sexual polyploidization and depolyploidization: some terminology and definitions. Theor Appl Genet **48:** 137–143

Mercier R, Vezon D, Bullier E, Motamayor JC, Sellier A, Lefèvre F, Pelletier G, Horlow C (2001) SWITCH1 (SWI1): a novel protein required for the establishment of sister chromatid cohesion and for bivalent formation at meiosis. Genes Dev **15:** 1859–1871

Murata T, Sonobe S, Baskin TI, Hyodo S, Hasezawa S, Nagata T, Horio T, Hasebe M (2005) Microtubule-dependent microtubule nucleation based on recruitment of gamma-tubulin in higher plants. Nat Cell Biol **7:** 961–968

Pastuglia M, Azimzadeh J, Goussot M, Camilleri C, Belcram K, Evrard JL, Schmit AC, Guerche P, Bouchez D (2006) Gamma-tubulin is essential for microtubule organization and development in *Arabidopsis*. Plant Cell **18:** 1412–1425

Peloquin SJ, Boiteux LS, Carputo D (1999) Meiotic mutants in potato: valuable variants. Genetics **153:** 1493–1499

Ramanna MS (1979) Re-examination of the mechanisms of 2n-gamete formation in potato and its implications for breeding. Euphytica **28:** 537–561

Ramsey J, Schemske DW (1998) Pathways, mechanisms, and rates of polyploid formation in flowering plants. Annu Rev Ecol Syst **29:** 467–501

Ravi M, Marimuthu MPA, Siddiqi I (2008) Gamete formation without meiosis in Arabidopsis. Nature **451:** 1121–1124

Reiser L, Fischer RL (1993) The ovule and the embryo sac. Plant Cell **5:** 1291–1301

Rhee SY, Somerville CR (1998) Tetrad pollen formation in quartet mutants of Arabidopsis thaliana is associated with persistence of pectic polysaccharides of the pollen mother cell wall. Plant J **15:** 79–88

Rhoades MM, Dempsey E (1966) Induction of chromosome doubling at meiosis by elongate gene in maize. Genetics **54:** 505–522

Ross KJ, Fransz P, Jones GH (1996) A light microscopic atlas of meiosis in Arabidopsis thaliana. Chromosome Res **4:** 507–516

Scott RJ, Spielman M, Bailey J, Dickinson HG (1998) Parent-of-origin effects on seed development in Arabidopsis thaliana. Development **125:** 3329–3341

Shimamura M, Brown RC, Lemmon BE, Akashi T, Mizuno K, Nishihara N, Tomizawa KI, Yoshimoto K, Deguchi H, Hosoya H, et al (2004) Gamma-tubulin in basal land plants: characterization, localization, and implication in the evolution of acentriolar microtubule organizing centers. Plant Cell **16:** 45–59

Vecchio AJD, Harper JDI, Vaughn KC, Baron AT, Salisbury JL, Overall RL (1996) Centrin homologues in higher plants are prominently associated with the developing cell plate. Protoplasma **196:** 224–234